Published in final edited form as:

Cancer Res. 2021 October 15; 81(20): 5336–5352. doi:10.1158/0008-5472.CAN-21-0483.

Oncostatin M Receptor-targeted antibodies suppress STAT3 signaling and inhibit ovarian cancer growth

Anjali Geethadevi[1,2,#], **Ajay Nair**[3,#], **Deepak Parashar**[1,2,#], **Zhiqiang Ku**[4,#], **Wei Xiong**[4], **Hui Deng**[4], **Yongsheng Li**[5], **Jasmine George**[1,2], **Donna M. McAllister**[6], **Yunguang Sun**[7], **Ishaque P. Kadamberi**[1,2], **Prachi Gupta**[1,2], **Michael B. Dwinell**[6], **William H. Bradley**[1], **Janet S. Rader**[1], **Hallgeir Rui**[7], **Robert F. Schwabe**[3,8], **Ningyan Zhang**[4], **Sunila Pradeep**[1,2,9], **Zhiqiang An**[4,*], **Pradeep Chaluvally-Raghavan**[1,2,9,*]

[1]Department of Obstetrics and Gynecology, Medical College of Wisconsin, Milwaukee, Wisconsin, 53226, USA.

[2]Medical College of Wisconsin Cancer Center, Medical College of Wisconsin, Milwaukee, Wisconsin, 53226, USA.

[3]Department of Medicine, Columbia University, 1130 St. Nicholas Avenue, New York, NY 10032, USA.

[4]Texas Therapeutics Institute, Brown Foundation Institute of Molecular Medicine, The University of Texas Health Science Center, Houston, Texas 77030, USA.

[5]Key Laboratory of Tropical Translational Medicine of Ministry of Education, College of Biomedical Information and Engineering, Hainan Medical University, Haikou 571199, China.

[6]Department of Microbiology and Immunology, Medical College of Wisconsin, Milwaukee, Wisconsin, 53226, USA.

[7]Department of Pathology, Medical College of Wisconsin, Milwaukee, Wisconsin, 53226, USA.

[8]Institute of Human Nutrition, Columbia University, 1130 St. Nicholas Avenue, New York, NY 10032, USA.

[9]Department of Physiology, Medical College of Wisconsin, Milwaukee, Wisconsin, 53226, USA.

[*]**Correspondence to** Zhiqiang An, Zhiqiang.An@uth.tmc.edu, Pradeep Chaluvally-Raghavan, pchaluvally@mcw.edu.
[#]These authors contributed equally to this work.

Authors Contribution

Conceptualization, P.C.-R., and S.P. Funding acquisition and Supervision, P.C.-R., S.P., N.Z., and Z.A. Experimental plan, P.C.-R., S.P., A.G., N.Z., and Z.A., Methodology and Investigation, A.G., D.P., A.N., P.C.-R., S.P, Z.K., M.B.D., N.Z., and Z.A., *In Vivo* and *In Vitro* Experiments, A.G., D.P., A.N., W.X., H.D., S.P, Z.K., I.P.K, Y.S., J.S., H.D., N.Z., and D.M., Bioinformatics, A.N., Y.L., and R.F.S., Clinical data analysis, W.B., J.S.R., and H.R., Data Analysis, A.G., Z.K., D.P., A.N., S.P., and P.C.-R., Figure Preparation, A.G., D.P., Z.K., and A.N., Writing – Original Draft, A.G., D.P., A.N., and S.P., P.C.-R., Writing – Review & Editing, A.G., J.S.R., H.R., S.P., Z.A., and P.C.-R.

Key resource table

List of all reagents and software used, along with their source information and research resource identifier numbers, is included in the Supplementary Data (Supplementary Table S6).

Data availability

The data that support the findings of this study are available from the corresponding author upon reasonable request.

Competing Interests: M.B.D. received non-financial support and other support from Protein Foundry, LLC and non-financial support and other support from Xlock Biosciences, LLC outside the submitted work. No potential conflicts of interest were disclosed by any other authors.

Abstract

While patients with advanced ovarian cancer may respond initially to treatment, disease relapse is common and nearly 50% of patients do not survive beyond five years, indicating an urgent need for improved therapies. To identify new therapeutic targets, we performed single cell and nuclear RNA-seq dataset analyses on 17 human ovarian cancer specimens, revealing the oncostatin M receptor (OSMR) as highly expressed in ovarian cancer cells. Conversely, oncostatin M (OSM), the ligand of OSMR, was highly expressed by tumor-associated macrophages and promoted proliferation and metastasis in cancer cells. Ovarian cancer cell lines and additional patient samples also exhibited elevated levels of OSMR when compared to other cell types in the tumor microenvironment or to normal ovarian tissue samples. OSMR was found to be important for ovarian cancer cell proliferation and migration. Binding of OSM to OSMR caused OSMR-IL6ST dimerization, which is required to produce oncogenic signaling cues for prolonged STAT3 activation. Human monoclonal antibody clones B14 and B21 directed to the extracellular domain of OSMR abrogated OSM-induced OSMR-IL6ST heterodimerization, promoted the internalization and degradation of OSMR, and effectively blocked OSMR-mediated signaling in vitro. Importantly, these antibody clones inhibited the growth of ovarian cancer cells in vitro and in vivo by suppressing oncogenic signaling through OSMR and STAT3 activation. Collectively, this study provides a proof of principle that anti-OSMR antibody can mediate disruption of OSM-induced OSMR-IL6ST dimerization and oncogenic signaling, thus documenting the pre-clinical therapeutic efficacy of human OSMR antagonist antibodies for immunotherapy in ovarian cancer.

Significance: This study uncovers a role for OSMR in promoting ovarian cancer cell proliferation and metastasis by activating STAT3 signaling and demonstrates the preclinical efficacy of antibody-based OSMR targeting for ovarian cancer treatment.

Keywords

anti-OSMR antibodies; IL6ST; ovarian cancer; scRNA-seq; STAT3

Introduction

Ovarian cancer (OC) is the most lethal gynecological malignancies and the fifth leading cause of cancer-related mortality in women in the United States. While patients with advanced ovarian cancer may respond initially to surgery, chemotherapy, and targeted therapy, many patients were reported with relapse of disease and nearly half of the patients do not survive beyond five years. (1–3). A recent study using single-cell RNA sequencing (scRNA-seq) of cells collected from the ascites samples of high-grade serous ovarian cancer (HGSOC) provided evidence for JAK/STAT3 signaling as a vulnerable target for ovarian cancer therapy (4). This study suggested that cells in the ascites fluid microenvironment, such as cancer-associated fibroblasts (CAFs) and tumor-associated macrophages (TAMs), express increased amount of gene transcripts encoding for ligands that activate JAK/STAT3 pathway. We and others have also shown that JAK/STAT3 pathway is an important signaling mechanism required for the growth and progression of ovarian cancer (5–8). Therefore, inhibiting STAT3 in cancer cells precisely has the potential to abrogate oncogenic signaling in cancer cells and eliminate or diminish their growth and metastasis. However, direct targeting of STAT3 with small molecule inhibitors such as JSI-124 showed suboptimal

potency, unfavorable pharmacokinetics (PK) properties, and non-specific effects in non-cancerous cells and immune cells (4). These adverse effects are also partly due to the high sequence similarity and homology between STAT transcription factors as well as the issues associated with poor bioavailability of STAT inhibitors (9).

It is known that the signaling outcome such as cell division and migration through IL6-family ligands is via the activation of Janus kinases (Jaks) and transcription factors of the STAT family (10). Upon stimulation by IL-6 subfamily of ligands such as IL6, IL11, ciliary neurotrophic factor (CNTF), leukemia inhibitory factor (LIF), oncostatin M (OSM), cardiotrophin 1 (CT-1), cardiotrophin-like cytokine (CLC), IL27 and IL31, the cytoplasmic tail receptor-associated kinases like JAK1, and JAK2 are phosphorylated and activated, which then serve as the docking sites for STAT transcription factors with matching SH2 domains primarily found in STAT3 and STAT1 proteins (6,11). Consequently, STAT proteins become phosphorylated and dimerize, then translocate to the nucleus and upregulate genes, which are important for cancer progression and metastasis (6,11). IL-6 family cytokines and their receptors constitute IL6R, IL11RA, ciliary neurotrophic factor receptor (CNTFR), leukemia inhibitory factor receptor (LIFR), oncostatin M receptor (OSMR), IL-27RA, and IL31RA. We hypothesize that inhibiting the selected IL6 family receptors that are predominantly expressed on cancer cells compared to stromal cells will suppress oncogenic signaling occurring through JAK/STAT3 pathway only in cancer cells.

Our analyses using single-cell RNA sequencing data from ovarian cancer cells obtained from patient ascites fluid revealed that OSMR has the potential to inhibit oncogenic STAT3-mediated oncogenic signaling in cancer cells. Signaling through OSMR is triggered by the binding of OSM to OSMR, which leads to heterodimerization of OSMR with interleukin-6 signal transducer (IL6ST; also known as glycoprotein 130 or GP130). OSM also binds to LIFR and causes its heterodimerization with IL6ST. Additionally, OSMR dimerizes with IL31RA, when IL31 binds to IL31RA (12). Studies were reported that OSMR as an important regulator for activating oncogenic pathways through JAK/STAT, MAPK, PKC isoforms and PI3K/AKT pathways in cancer cells (13,14). However, OSMR as a potential therapeutic target for ovarian and other cancers has not been explored. Monoclonal antibodies (mAb) targeting cell surface receptors on cancer cells such as EGFR, ERBB2 (HER2), and VEGFR2 have been successfully developed as therapies for the treatment of multiple solid tumors (15–17). To develop therapy against OSMR, we developed a novel set of OSMR-targeted monoclonal antibodies by panning phage-displayed scFv human antibody libraries against the extracellular domain of human OSMR and examined their effects on proliferative and metastatic properties of ovarian cancer cells.

Materials and Methods

Patient samples and Cell lines

Ovarian cancer tissue and Normal ovarian tissue samples were obtained from Cancer Center and Department of Obstetrics & Gynecology, Froedtert Hospital, Medical College of Wisconsin after approval by the Institutional Review Board (IRB) of Medical College of Wisconsin. All human samples were collected with written informed consents from patients under an Institutional Review Board (IRB) of Medical College of Wisconsin approved

protocol in accordance with recognized ethical guidelines of Declaration of Helsinki. Cell lines included and their sources are described in the supplementary methods. All cell lines were used between passages 3 and 25. Cell line authentication was performed by short tandem repeat (STR) profiling at the IDEXX Bioanalytic Laboratories Inc (Westbrook, Maine, USA), and tested as mycoplasma negative by PCR (Agilent Mycosenser Mycoplasma assay kit) as recent as two months prior to last experiments.

Single cell/nucleus RNA-seq analysis

A total of 17 human ovarian cancer samples from single cell/nucleus RNA-seq data were analyzed in this study. The datasets OvD1–10x, OvD2–10x and OvD3–10x-nuc were single-patient ovarian cancer samples. The first two datasets were 10x droplet-based single cell RNA-seq (scRNA-seq) and the third was 10x droplet-based single nucleus RNA-seq (snRNA-seq) data. These were obtained from (4) with GEO accession no. GSE140819 (GSM4186985, GSM4186986 and GSM4186987, respectively). The raw counts matrix in h5 format and their corresponding cell annotations in metadata files were used for the analysis. The datasets OvD4–10x-mult and OvD5-SS2 were multi-patient ovarian cancer samples with n=6 (but 8 samples with multiple temporal sampling) and n=9, respectively. But one patient was common in OvD4–10x-mult and OvD5-SS2 dataset. The first dataset was 10x droplet-based scRNA-seq and the second was plate-based high-depth SMART-seq2 (SS2) scRNA-seq. The log-tpm-normalized data and the annotation were obtained from (18) with GEO accession no. GSE146026.

Tissue microarray (TMA) and immunohistochemistry (IHC)

Formalin-Fixed Paraffin-Embedded (FFPE) tissue array cores (OV1005bt and OV1004) consisting of 5μm tissue sections from ovarian cancer patients, normal and normal adjacent ovarian tissue sections were procured from US Biomax Inc (Rockville, MD). See Supplementary-Table. S1 for TMA dataset information. For the expression of proteins in the tissues sections from tumor bearing mice, the tissues were fixed overnight in formalin jars and sections were paraffin embedded. Hematoxylin and eosin (H& E) staining was used to counterstain the tissues from all treatment groups.

TMA was performed as previously mentioned (19). Protein expression was represented by IHC score (0–5) was calculated for each section by adding the score of percentage of positive cells (intense red staining) (0 ≤ 5%, 1 = 6–20%, 2 = 21–40%, and 3 = 41–60%, 4=61–80%, 5=81–100%) and the intensity score: 0 (negative), 1 (weak), 2–3(moderate), and 3.1–4 (high) and 4.1–5 (very high).

Gene silencing, Ectopic Expression, Real-time PCR and qPCR analysis

Total RNA was extracted using RNAeasy kit (Qiagen) and quantified on Nanodrop 2000 (Thermo Scientific) as described previously. One microgram of total RNA was reverse transcribed using iScript Reverse Transcription Supermix for RT-qPCR (Bio-Rad). Real-time PCR was performed with iTaq Universal SYBR Green Supermix (Bio-Rad) according to manufacturer's instructions using a Bio-Rad CFX Connect Real Time PCR system (Bio-Rad). The abundance of mRNA was determined using the ΔΔCT method (where Cq is threshold cycle). mRNA expression was normalized to β-Actin (ACTB) mRNA.

Sequences of the primers used are shown in Supplementary Table. S2. Silencing or overexpression of genes were performed as described previously (5). siRNAs and the plasmids were transfected at a concentration of 5nM to 20 nM using RNAi max (Invitrogen) (Supplementary Tables. S3 and S4).

Ligand-receptor interaction analysis

CellPhoneDB (20) is a curated repository of interactions between ligands and receptors along with the molecular subunit architecture information. These details are integrated in a statistical framework to infer cell-cell communication network in single-cell transcriptomics data. CellPhoneDB v.2.0.0 was used and the recommended procedures for preparation of input files (20) were followed. Briefly, the log-normalized gene expression data and the metadata of cell type identities (obtained previously with clustering and cell-type specific markers) were used as the input. Ligand-receptor interactions were then identified using 'cellphonedb method statistical_analysis' command with default parameters. The interactions were visualized using ggplot2 R package.

Phage library panning of antibodies to the OSMR

The OSMR protein (Sino Biologicals, 11226-H08H) was used for antibody selection by panning a large human scFv phage display antibody library. The library was constructed in house from the cDNA extracted from the PBMCs and tonsils of multiple donors. In each round of phage panning, 50μg of protein was coated on a MaxiSorp immune tube and blocked by 8% milk. The phages were pre-blocked by 8% milk then incubated with the antigen pre-coated on the immune tube. After washing with PBST and PBS, the phages were eluted by triethylamine (TEA). The eluates were tittered and infected *E. coli* TG1 for phage amplification for next round of panning. Similar procedures were performed in round 2 of panning with increased washing stringency. After 2 rounds of panning, the phage eluates were used to infect *E. coli* TG1 to grow single colonies for picking by QPix420 system (Molecule Devices) and for phage preparation.

Phage ELISA

A total of 1504 single colonies were picked to make phage for ELISA binding with OSMR. ELISA plates were coated with OSMR antigen at 1μg/mL in PBS for overnight at 4℃. The plates were blocked with 5% milk for 2 hours at 37℃ and the phages were pre-blocked with 5% milk for 1 hour at room temperature. After blocking, the phages were added into the wells of the ELISA plates and incubated for 2 hours at 37℃. An HRP-conjugated Mouse-anti-M13 secondary antibody was 1:1000 diluted in 5% milk and added into the wells for incubation for 1 hour at 37℃. The plates were washed 3 times between each incubation steps and 5 times before color development. The TMB substrate was added into the wells (100μl/well) for color development for 5 mins. The H_2SO4 was used to stop the reaction.

IgG expression and purification

A total of 500 phage clones which were positive in the phage ELISA were sequenced for the scFv regions. After analysis of the complementarity-determining regions (CDRs), 35

scFvs with unique amino acid sequences were obtained and further subjected to conversion into full IgG1 heavy chain and light chain constructs. These constructs were co-transfected Expi293 cells for expression of recombinant antibodies according to manufacturer's instructions. After 7 days, antibodies were purified by affinity chromatography using protein A resin. A total of 26 antibodies were produced for further experiments.

Affinity measurement with BLI

For antibody affinity measurement, antibody (20 μg/mL) was loaded onto the protein G biosensors for 150s. Following a short baseline in kinetics buffer, the loaded biosensors were exposed to a series of recombinant OSMR concentrations (0.41–900 nM) and background subtraction was used to correct for sensor drifting. All experiments were performed with shaking at 1,000 rpm. Background wavelength shifts were measured from reference biosensors that were loaded only with antibody. ForteBio's data analysis software was used to fit the data to a 1:1 binding model to extract an association rate and dissociation rate. The Kd was calculated using the ratio koff/kon.

Animal studies

All animal work was done in accordance with protocol approved by the Institutional Animal Care and Use Committee (IACUC) at the Medical College of Wisconsin. To compare the ability of OSM, LIF and IL31 on ovarian cancer growth, HEYA8-Luc+ cells were treated with vehicle/PBS (control), OSM (100ng/mL), LIF (100ng/mL) and IL31 (50ng/mL) *in vitro* for 24h and subcutaneously (s.c) injected (1×10^5 cells/animal) into 4–6 weeks old athymic female nude mice (Nu/Nu) (Envigo, Madison, WI, USA) per flank. The mice were treated intraperitoneally (i.p) with PBS, OSM (250ng/kg b.w), LIF (250ng/kg b.w) and IL31 (250ng/kg b.w) twice a week for total of 4 weeks.

To study the effect of stable knockdown of OSMR on the ovarian cancer tumor progression, shOSMR#1-Heya8-Luc+ cells (3×10^4 cells/animal) and shControl-HEYA8-Luc+ cells were intraperitoneally injected into 4–6-week-old athymic female nude mice (Nu/Nu) (Envigo, Madison, WI, USA) (N=7/ group) with a 27-gauge needle. Athymic female nude mice (Nu/Nu)) bearing Heya8-Luc+ cells (3×10^4 cells/animal) were treated with Control IgG, B14 mAb, or B21 mAbs (10 mg/kg body weight) with or without OSM (250ng/kg b.w) twice a week for five weeks to determine the efficacy of anti-OSMR antibodies. Mice were monitored for tumor growth once every week by bio-luminescence imaging using Xenogen IVIS100 imaging system (Caliper Life Sciences Inc, Waltham, MA). All mice were euthanized at the end of 5 weeks or when moribund. Tumors were harvested and weighed, total number of tumor nodules and metastasis to distant organs were counted and imaged using IVIS100. The tumors were excised and then proceeded for IHC, Western blotting and qPCR. Serum was collected from both groups for OSM ELISA. Tumor volume was calculated by the formula V = (W (2) × L)/2 in the respective groups.

To study the levels of Osm in ascitic fluid, BR-Luc murine cell lines (1×10^6 cells/mouse) stably knockdown with shOsmr and shControl were intraperitoneally injected into 4 to 6 weeks old female FVB/NJ-Homozygous syngeneic mice model (Charles River Laboratories, Wilmington, MA, USA) (N=6) with a 27-gauge needle. Mice were monitored for tumor

growth once every week by bio-luminescence imaging using Xenogen IVIS100 imaging system. All mice were euthanized at the end of 6 weeks or when moribund. Ascites were collected in complete media and cells from ascites were filtered using 40μm filter. To collect the cells from non-tumor bearing control mice and shOSMR-BR-Luc mice, 1 to 3 ml of sterile PBS was flushed in the peritoneum (peritoneal wash) and filtered using 40μm filter. The filtrate containing cells were centrifuged at 1500 rpm and the pellet was washed with PBS.

Annexin V/PI apoptosis assay

HEYA8 and OVCAR4 cells were collected, washed in cold PBS and stained using FITC Annexin V/Dead Cell Apoptosis Kit (BD Pharmingen) as described previously as per manufacturer's guidelines (21). Labeled cells were detected in LSR II Flow Cytometer (BD Biosciences). The data were analyzed using FlowJo Software (FlowJo LLC).

Flow sorting

Cell sorting was performed as described previously (21) with some modifications. The cell pellet from ascites of tumor bearing mice and healthy controls were prepared for FACS by removing dead cells using Dead cell removal kit (Miltenyi Biotech, San Diego, CA) followed by staining with Brilliant Violet 510™ anti-mouse CD45 for immune cells, APC anti-mouse CD140a (PDGFRα) for fibroblasts, Alexa Fluor® 488 anti-mouse F4/80 for macrophages, and PE anti-mouse CD136 (EpCAM) for tumor cells. Stained cells were immediately sorted from single-cell suspension using BD FACS Aria™ III Cell Sorter (BD Biosciences, New Jersey, USA). CD45+F4/80+ macrophages, CD45-CD140a+ fibroblasts, -CD45-EpCAM+ tumor cells and epithelial cells were collected from tumor bearing mice and non-tumor bearing control mice. Cell pellets collected from each population were centrifuged at 1500rpm at 4°C and proceeded for RNA isolation and qPCR analysis to check Osm levels in both groups.

Cell viability assay and Receptor internalization using Live Cell Incucyte Analyzer

The IncuCyte® Live Cell imaging system (Essen BioScience, Ann Arbor, MI) (22) was used for assessment of cell viability. Briefly, 10^4 cells were seeded in quadruplicates in a 96-well plate containing complete medium. Following serum starvation, the cells were treated with Control IgG (10μg/mL) or OSM (100ng/mL) stimulation with or without anti-OSMR antibodies (10μg/mL) and incubated with 1:200 dilution of IncuCyte® Annexin V Red Reagent (Essen Bioscience). Cell viability was measured in real-time using the IncuCyte by taking 3 field images per well every 6 h for a period of 48h. Red cell counts based on number of red apoptotic cells were performed using IncuCyte® S3 Software (Essen Bioscience).

For receptor internalization, anti-OSMR antibodies B14 and B21 or isotype control IgG (10μg/mL) were labeled with pH sensitive FabFluor (Red) reagent (Essen Bioscience) as per manufacturer's instructions and added to serum starved ovarian cancer cells in the presence of OSM (100ng/mL). The cells were then monitored in IncuCyte Live Cell Analysis system for 24h. The antibody labeled with FabFluor Red reagent is non-fluorescent at neutral pH (outside cell). In due course, if the antibody-receptor complex gets internalized, antibody

labeled with pH sensitive dye fluoresce red in the form of clusters inside cytoplasm due to acidic pH of endosomal and lysosomal compartments which is then analyzed using the IncuCyte® S3 Software.

Western blot analysis and protein array

Cells were washed twice in ice-cold PBS and lysed in RIPA buffer (150 mM NaCl, 0.1% SDS, 1% NP-40, 1% sodium deoxycholate) (Santa Cruz Biotechnologies) supplemented with protease inhibitor cocktail (Sigma Aldrich) and Western blot was performed as mentioned previously (5). A Proteome Profiler Human Apoptosis Array Kit (Cat# ARY009; R&D Systems) was used to analyze apoptosis-related protein profiles and Human Phospho-Kinase Antibody Array kit (Catalog # ARY003B; R&D Systems) was used to analyze proteins phosphorylated by OSM or inhibition of phosphorylation by anti-OSMR antibodies according to manufacturer instructions. In brief, the total protein isolated from OVCAR4 cells after treatment with Control IgG (10μg/mL), OSM (100 ng/mL) and anti-OSMR antibodies B14 and B21 (10μg/mL each) in the presence of OSM for 60 min (Protein kinase array) and for 48h (Apoptosis array) were first incubated with the array membrane overnight at 4°C, followed by incubation with a biotinylated detection antibody cocktail at room temperature for 1 h. The membranes were then exposed to X-Ray film and quantified by Image J software (National Institutes of Health, Bethesda, USA).

Receptor Dimerization assay

Dimerization assay was performed as mentioned previously (23,24) with some modifications. HEYA8 and OVCAR4 cells were seeded overnight and upon 70–80% confluency, serum starved overnight and pre-treated with Control IgG, B14 and B21 mAbs (10μg/mL) then stimulated with OSM (100ng/mL) for 60min on ice to prevent internalization of dimerized receptors. The cell lysates were incubated with non-permeable cross-linking reagent, 3mM bis (sulphosuccinimidyl) suberate [BS3], cross-linking reagent on ice for 30min and subsequently quenched with 250mM Glycine. The cells were washed with ice cold PBS and cells were lysed using RIPA buffer as mentioned earlier. The pre-cleared lysates were immunoprecipitated overnight at 4°C using anti-OSMR antibody bound to Dynabeads (Thermo Fisher Scientific) and eluted using 1x Laemmli sample buffer and the proteins were separated on a 6% SDS/PAGE. Separated proteins were transferred to PVDF membrane and immunoblotted with OSMR, IL6ST or IL31RA antibodies.

Receptor internalization

Receptor internalization was performed as mentioned previously (25) with some modifications. Briefly, cells were seeded in 100mm culture dish and once adhered, cells were serum starved for 16h and treated with Control IgG and anti-OSMR antibodies (10μg/mL each) in the presence of OSM (100ng/mL) for 6 h. Cells were washed with ice cold PBS and membrane and cytosolic protein fractions were isolated using Mem-PER™ Plus Membrane Protein Extraction Kit (Thermo Fisher Scientific) according to manufacturer's guidelines. Protein concentration in each fraction was determined using BCA kit and the 30μg protein lysates from each fraction was separated by 8% SDS-PAGE.

On-Cell Western assay

On-cell western blot was performed as described earlier (26) with some modifications. Briefly, cells were seeded on 96 well (black plate) at a density of 5×10^3 cells per well for HEYA8 and 1×10^4 cells for OVCAR4. Following serum starvation, cells were treated with B14 and B21 antibodies (10μg/mL each) along with OSM (100ng/mL). Cells were also treated with Isotype control IgG (10μg/mL each) with and without OSM (100ng/mL) for 16h and washed with ice cold PBS and fixed with 4% paraformaldehyde. The cells were blocked for 1 h in LICOR blocking buffer and incubated with primary antibody against extracellular domain of OSMR (1:100 dilution, Cat: 11226-RP02 Sino Biologicals, Wayne, PA) along with Na,K-ATPase antibody (Santa Cruz Biotechnologies) overnight at 4^{O}C. The cells were further washed with PBS and incubated with secondary antibodies IRDye® 680RD Donkey anti-Rabbit IgG Secondary Antibody (Red) (1:800 dilution) and IRDye® 800CW Goat anti-Mouse IgG Secondary Antibody (Green) (1:200 dilution) (LI-COR, Lincoln, Nebraska) for 1h and developed in Odyssey Scanner (LI-COR). The fluorescence intensity was quantitated using Li-Cor image studio software.

Immunofluorescence

OVCAR4 cells (5×10^4 cells) were treated with control IgG, B14 and B21 (10μg/mL each) and stimulated with OSM (100ng/mL) on coverslip for 16h. Cells were fixed with 4% paraformaldehyde for 10 min and permeabilized with 0.1% triton for 5 min. Cells were then incubated with OSMR (Proteintech) and LAMP1 (Cell Signaling Technology) primary antibodies overnight at 4ºC followed by incubation with goat anti-rabbit Alex Fluor 488 (green) and goat anti-mouse Alexa Fluor 546 secondary antibodies for 1h at room temperature. Cells were mounted with DAPI containing mounting media (Thermo Fisher Scientific) and visualized in Zeiss LSM 510 confocal microscope.

Cytokine ELISA

The levels of OSM in serum were determined by human OSM ELISA kit (R&D systems) according to manufacturer's guidelines and as previously mentioned (5). Blood was collected from tumor-bearing mice were allowed to clot for 30 min at room temperature, before being centrifuged at 16,000×g for 10 min and serum was aspirated. Briefly, human OSM antibody provided with the kit was pre-coated onto microwells. Human OSM present in the sample or standard binds to antibodies adsorbed to the microwells. Following incubation, unbound biological components were removed during a wash step. A biotin-conjugated anti-human OSM antibody that binds to human OSM primary antibody was added first. Following incubation unbound biotin- conjugated anti-human OSM antibody is removed during a wash step. Streptavidin HRP was added that binds to the biotin-conjugated anti-human OSM antibody. A colored product formed in proportion to the amount of human OSM present in the sample or standard was detected by addition of substrate and absorbance is measured at 450 nm.

Ascitic fluid and peritoneal wash were collected from FVB mice injected with shControl-BR-Luc and shOsmr-BR-Luc cells respectively and levels of OSM were detected by mouse OSM ELISA kit (R&D systems) according to manufacturer's guidelines.

Gene set enrichment analysis

For Gene set enrichment analysis (GSEA), gene expression data of ovarian cancer was obtained from TCGA project. The expression of genes was measured by fragments per kilobase of exon model per million reads mapped (FPKM). We first calculated the Pearson Correlation Coefficient (PCC) between the expression of genes and OSM or OSMR. All genes were ranked based on PCC and then subjected to GSEA analysis (27). Enrichment score (ES) was calculated for each functional set, which reflects the degree to which a gene set is overrepresented at the top or bottom of the ranked list of genes. The normalized enrichment score (NES) was calculated based on 1000 permutations. Here, the cancer hallmark gene sets from MSigDB were considered and the gene sets with false discovery rate <0.001 were considered as a selection criterion (27,28).

Statistical analysis

Cell culture-based experiments were repeated at least three times (three biological replicates) and all data were expressed as means ± SE. Significance was assessed by unpaired two-tailed Student's t-test using GraphPad Prism. Comparison analysis between two treatment groups in animal models was performed by One-way ANOVA followed by Dunnett's multiple comparison test. Statistical analysis of the animals treated in the survival model was done by a log-rank (Mantel–Cox) test. The differences were considered to be statistically significant for P-values <0.05 (*), <0.01 (**), <0.001 (***), and <0.0001 (****).

Results

OSMR is differentially expressed in ovarian cancer cells and in cancer associated fibroblasts

To identify targetable IL6 family receptors that are differentially expressed in ovarian cancer cells and cancer associated cells, we analyzed droplet-based three single-cell RNA sequencing (scRNA-seq) datasets (OvD1–10x, OvD2–10x and OvD4–10x-mult) (Supplementary Fig. S1-S4) and one single-nucleus RNA sequencing (snRNA-seq) dataset (OvD3-nuc) of human ovarian cancer patient samples (Supplementary Fig. S3) (4,18) and determined the expression of all IL6 family receptors such as IL6ST, OSMR, IL27RA, LIFR, IL11RA, IL6R, CNTFR, and IL31RA. There were 9 patients and 11 samples in these droplet-based datasets (Supplementary Fig. S1-S6), where we found OSMR and its dimerizing partner IL6ST among the top highly expressed receptors in ovarian cancer cells, cancer associated fibroblasts and endothelial cells compared to immune cells (Fig. 1A-B and Supplementary Fig. S1 to S6).

Although, droplet-based scRNA-seq and snRNA-seq have high sequencing coverage, however, both approaches exhibit some limitations because of high chances of dropout of genes due to low-depth coverage in sequencing (29). Therefore, we used a plate-based, low dropout and high-depth SMART-seq2 (SS2) scRNA-seq data (OVD5_SS2) from n=9 human ovarian cancer patients (Fig. 1C-1D and Supplementary Fig. S6A) and confirmed our results from 10X datasets. Our analysis again confirmed that OSMR and IL6ST are the top highly expressed IL6 family receptors in cancer cells. We also observed that OSMR is highly

expressed in ovarian cancer cells and cancer associated fibroblasts, and in a lesser degree in macrophages (Fig. 1E-F and Supplementary Fig. S5A). Notably, we found that OSM, which is the ligand of OSMR, is mainly produced by macrophages (Fig. 1F and Supplementary Fig. S1 to S6).

Next, we determined all the known ligand-receptor interactions between different cell types in OvD5-SS2 dataset using CellPhoneDB (20) (Supplementary Material. 1) and selected all the interactions involving IL6 family ligands and their receptors (Fig. 1G). Here, we found that OSMR, IL6ST, LIFR, IL11RA and IL6R showed significant cell-cell interactions with their ligands expressed by macrophages and fibroblasts.

However, LIFR and IL11RA are expressed in very few ovarian cancer cells (Fig. 1 E-F and Supplementary Fig. S6C), whereas IL6R is ubiquitously expressed in all cell types and particularly high in immune cells (Fig. 1A, 1E, Supplementary Fig. S6E). Notably, IL6ST is also expressed highly in all cell types, whereas its dimerizing partner OSMR is highly expressed predominantly in ovarian cancer cells, tumor associated endothelial cells and fibroblasts (Fig. 1A, 1E-F). Our analysis further showed that IL6ST interacts with multiple IL6 family ligands such as OSM, IL6, and IL11 as demonstrated in Fig. 1G, which leads to the dimerization of IL6ST with multiple IL6 family receptors such OSMR, LIFR, IL6R, and IL11RA (Fig. 1G), CNTFR, and IL27R (6) (Fig. 1G). Strikingly, we found that OSMR interacts with only OSM (Fig. 1G) and heterodimerizes with IL6ST (Fig. 1G). Though IL6ST is highly expressed in ovarian cancer cells (Fig. 1A, 1B and 1G), its ability to dimerize with multiple chemokine and cytokine receptors for vital functions of immune cells limits its potential as a highly specific cancer target. Thus, we decided to characterize and focus on the functions of OSMR, which is the second most and highly expressed IL6 family receptor in ovarian cancer cells as a therapeutic avenue to treat ovarian cancer (Fig. 1A, 1B).

OSM-signaling through OSMR is a critical mechanism for pathological characteristics of ovarian cancer

We then examined the protein levels of OSMR subfamily of receptors which include IL6ST, LIFR, IL31RA and OSMR in a panel of ovarian cancer cell lines and found that OSMR is highly upregulated in most of the aggressive ovarian cancer cells as compared to fallopian tube epithelial cells such as FTE cell lines and normal ovarian surface epithelial cells (OSE) whereas IL6ST receptor is also highly expressed in most of the cell lines, however there is no significant changes in the expression between FTE, OSE and ovarian cancer cells. (Fig. 2A and Supplementary Fig. S7A and S7B). In conjunction with our single cell analysis results, we found that LIFR and IL31RA are poorly expressed in ovarian cancer cell lines (Fig. 2A and Supplementary Fig. S7A and S7B).

To further validate OSMR and IL6ST are critical for oncogenic signaling in ovarian cancer cells, we determined the protein expression of all the OSMR subfamily receptors (OSMR, IL6ST, IL31RA and LIFR) and other IL6 family receptors, in ovarian cancer tissues and adjacent normal tissue. We found that OSMR is highly and differentially expressed in cancer tissues compared to normal adjacent tissues (NAT); whereas we noticed that IL6ST is highly expressed in all samples and not differentially expressed between normal ovarian tissues, NAT and ovarian cancer tissues (Fig. 2B and Supplementary Fig. S7C to S7E). Similar to the

single cell/nucleus RNA-seq datasets, we found that LIFR is poorly expressed and there is no change in its level between NAT and cancer tissues. We further found IL31RA has little or no expression in both normal and ovarian cancer tissues (Fig. 2B and Supplementary Fig. S7C to S7E). Next, we determined the effect of secreted OSM on dimerization of OSMR with itself and with IL6ST, which is the first process for oncogenic signaling in ovarian cancer and found that OSM stimulation improved the dimerization between OSMR-OSMR and OSMR-IL6ST in OVCAR4 and HEYA8 ovarian cancer cells (Fig. 2C).

Intriguingly, increased expression of OSMR in fibroblasts, and endothelial cells in ovarian cancers (Fig. 1A, 1B and 1E), suggest that the association of above cells with tumor cells could upregulate OSMR expression in tumor associated fibroblasts, macrophages and endothelial cells. To confirm this hypothesis, we determined the mRNA expression of OSMR family receptors in fibroblasts, macrophages (THP1) and endothelial cells (RF24) that were either grown alone or co-cultured with normal ovarian epithelial cells (OSE) and ovarian cancer cells (HEYA8 and OVCAR4). Strikingly, we found that both OSMR and IL6ST were upregulated highly in endothelial cells and fibroblasts, and modestly in macrophages when co-cultured with ovarian cancer cells compared to the cells when cultured alone or co-cultured with OSE cells (Supplementary Fig. S7F); whereas we observed low to modest change in the expression of IL31RA expression in fibroblasts, macrophages and endothelial cells when co-cultured with ovarian cancer cells. We further observed that LIFR and IL6R were upregulated highly in endothelial cells and macrophages respectively, when co-cultured with cancer cells.

To further confirm the importance of OSM family receptors on oncogenic characteristics in both ovarian cancer cells and the cells in TME, we knocked down all the IL6 subfamily genes in ovarian cancer cells, and cells in TME such as fibroblast, endothelial (RF24) and macrophage (THP1) cells and determined cell proliferation and migration. Here, we found that the loss of OSMR considerably reduced the proliferation (Supplementary Fig. S8A) and migration (Supplementary Fig. S8E) in ovarian cancer cells (>70%) but did not exert any major effects on the proliferation and migration of non-cancer cells (Supplementary Fig. S8B to S8D and S8F to S8H). We further observed that the knockdown of IL6ST and IL6R reduced the proliferation and migration of ovarian cancer cells low to modest levels compared to the knockdown of OSMR (Supplementary Fig. S8A, S8B, and S8E), whereas we noticed that the loss of IL6ST and IL6R inhibited the proliferation and migration of fibroblast, endothelial and macrophage lines significantly (Supplementary Fig. S8B to S8D and S8F to S8H). Taken together our data demonstrate that OSMR is an important regulator of ovarian cancer cell proliferation and migration compared to other IL6 family receptors.

Our Gene Set Enrichment Analysis (GSEA) (28) further showed that high levels of OSM and OSMR are associated with functional annotation marks such as epithelial-to-mesenchymal transition and IL6/JAK/STAT3 signaling pathways in the TCGA ovarian cancer cohort (Fig. 2D and Supplementary Fig. S9A). In conjunction, immunohistochemistry (IHC) using tissue microarrays (TMAs) consisting of 110 ovarian tumors (Supplementary Table. S1) exhibited high OSMR expression in the high-grade serous ovarian cancer patient samples compared to the low-grade serous ovarian cancer (Fig. 2E and 2F). We also noticed that OSMR is highly expressed in the malignant stage

I, II and III ovarian cancer tissues compared to normal and NAT tissues (Fig. 2G and 2H) whereas we did not find any stagewise difference in OSM expression in ovarian cancer tissues (Supplementary Fig. S9B). We also found that OSM increased the spheroid forming ability and size of ovarian cancer spheroids compared to IL31 and LIF in our 3-dimensional cultures (Fig. 2I and Supplementary Fig. S9C). Importantly, OSM stimulation prolonged the phosphorylation at both Y705 and S727 moieties of STAT3 compared to LIF and IL31 in HEYA8 ovarian cancer cells (Fig. 2J and 2K). In conjunction, OSM promoted the growth of HEYA8 cancer cells rapidly compared to LIF and IL31 treatment *in vivo* (Fig. 2L, 2M and 2N).

To investigate the downstream effects of OSMR activation upon OSM in ovarian cancer cells, we stimulated OVCAR4 cells which express high levels of OSMR with recombinant human OSM and performed phospho-proteomic array and determined the phosphorylation of 45 proteins. In this assay, we found that OSM stimulation increased the phosphorylation of several key proteins including CREB, ERK, STAT3, Akt, p70s6kinase, where pSTAT3-Y705 was the most upregulated phosphoprotein (Supplementary Fig. S10A and S10B). We also characterized the oncogenic effects of OSMR by overexpressing OSMR in HEYA8 and OVCAR5 ovarian cancer cells using the pUNO1-OSMR plasmid. First, we performed immunoblot using lysates of cells overexpressing OSMR and found a substantial increase in the phosphorylation of Y705 and S727 moieties of STAT3 upon OSMR overexpression (Supplementary Fig. S10C and S10D). OSMR also promoted colony formation, migration, invasion, wound healing ability and the spheroid forming capability in both cell lines (Supplementary Fig. S10E to S10J).

Knock down of OSMR reduced oncogenic characteristics and inhibited the growth and metastasis of ovarian cancer cells

Next, we determined if the knockdown of OSMR reduce the phosphorylation of STAT3 and the growth, migration and invasion of cancer cells. We found that shRNA-mediated depletion of OSMR reduced phosphorylation of STAT3 at S727 and Y705 moieties (Supplementary Fig. S11A and S11B). We next determined if OSMR is required for the effects of OSM. In contrast to the effect of OSM in control cells, OSM stimulation could not activate the phosphorylation of STAT3 in the cells that were stably knocked down with shOSMR (Supplementary Fig. S11B). Similarly, OSM stimulation did not induce any effect on spheroid formation, colony forming ability, cell migration or invasion in the cells that were knocked down with shOSMR, which again confirmed that OSMR is required for the effects of OSM (Supplementary Fig. S11C to S11E).

To determine the effects of loss of expression of OSMR on ovarian cancer growth *in vivo*, we injected luciferin labeled shControl-HEYA8 cells or shOSMR-HEYA8 cells intraperitoneally in nude mice (n=7 mice/group) and monitored the growth of cancer cells by bioluminescent imaging using *in vivo* imaging system (IVIS) up to 5 weeks (Fig. 3A and 3B). Our IVIS imaging in live animals showed that OSMR knockdown inhibited ovarian cancer cell growth by approximately 70% specifically in the last two time points (Fig. 3B and 3C). In conjunction, we also found that silencing of OSMR markedly reduced the tumor weight and tumor burden as well as incidence of metastasis at various organ sites

including omentum, peritoneum, perihepatic, perisplenic and pelvic sites (Fig. 3D to 3F). Consistent with the results that OSMR knockdown inhibited the ovarian cancer growth, our IHC and immunoblot analysis showed that the stable knockdown of OSMR in these mice significantly decreased the cell proliferation marker Ki67 and increased the levels of apoptosis marker cleaved caspase-3 (Fig. 3G to 3I). Notably, loss of OSMR also led to a decrease in the levels of proliferation marker PCNA and anti-apoptotic markers BCL-xl and BCl2 compared to the respective controls (Fig. 3I). Next, we checked the levels of secreted OSM in serum collected from the mice bearing HEYA8-control or HEYA8-shOSMR tumors and observed a significant reduction in the OSM levels in the serum collected from the mice bearing HEYA8-shOSMR tumors compared to the control (Fig. 3J). We also found that the loss of OSMR mRNA expression resulted a loss in the levels of phosphorylated STAT3 compared to sh-control (Fig. 3G to 3K and Supplementary Fig. S11F).

HEYA8 tumors rarely develops ascites in mice; thus, we used a murine ovarian cancer cell line BR-Luc which develops ascites to study the effect of OSMR on OSM levels in ascitic fluid. Notably, the depletion of OSMR resulted into no ascitic fluid or very little ascites compared to the control group. To compare the levels of OSM in peritoneum, we quantitated OSM either in the ascites fluid or in the peritoneal wash of those mice with no ascites and found that the mice bearing OSMR-depleted cells expressed poor amount of OSM in the peritoneal wash (Supplementary Fig. S11G). In conjunction with the single cell analysis of clinical samples of ovarian cancer (Fig. 1F and Supplementary Fig S1 to S6), we found that the macrophage populations compared to epithelial cells and fibroblast expressed high levels of OSM in both peritoneal wash and ascites fluid of BR-Luc tumor bearing mice (Supplementary Fig. S12A to S12D). Taken together, our results demonstrate that OSMR-depletion inhibited STAT3 phosphorylation, OSM levels and subsequent tumor growth.

Development and screening of anti-OSMR antibodies that inhibit the growth of ovarian cancer cells

Given that OSMR is highly and differentially expressed in cancer cells, we sought to develop a monoclonal antibody against OSMR to inhibit the growth and progression of ovarian cancer. Towards this aim, we panned a phage displayed single-chain variable fragment (scFv) antibody library against the extracellular domain of OSMR and selected all the positive scFv antibody clones which binds to recombinant OSMR upon screening in antigen-specific binding hits by ELISA. The scFv clones that exhibited high binding affinity to OSMR were then converted to full-length IgG1 antibodies (Fig. 4A).

All the positive 26 full-length antibody clones, that have markedly high binding affinity towards extracellular domain of OSMR were identified and screened for their effect on ovarian cancer cell viability after treating the cancer cells with 10μg/mL of antibody in the presence of OSM at multiple time points up to 48h (Fig. 4B). We used WP1066, a potent inhibitor of STAT3 as a positive control and control IgG as an Isotype control (Fig. 4C). In our screening, we observed that three antibodies named B14, B18, and B21 are the most potent antibodies that induce apoptosis in OVCAR4 cells even when grown in the presence of OSM (Fig. 4C, 4D and Supplementary Fig. S13A). Next, we determined the cell

viability upon B14, B18, and B21 antibody treatment in OVCAR4 cells using CCK8 cell viability assay and found that the IC50 of B14, B18, and B21 antibody clones are ~10μg/mL (Supplementary Fig. S13B). Then, we analyzed the binding affinity of these antibodies to cell surface human OSMR protein by ELISA and found that antibodies B21 and B14 exhibited an effective concentration 50% (EC50) at 1.45 and 1.17 nM for B14 and B21 antibody respectively. Unexpectedly, B18 antibody clones did not show any specific binding to OSMR (Fig. 4E). Thus, we focused on B14 and B21 antibodies to further characterize their effects on cellular signaling, tumor growth and metastasis. Importantly, both B14 and B21 treatment reduced the levels of phosphorylation of pSTAT3 (S727 and Y705), pAkt, p70s6Kinase, WNK1, PYK2, RSK1/2/3 and PLC-1 proteins our phospho-protein kinase array, where B21 was more effective on inhibiting those oncogenic kinases (Fig. 4F). We also noticed that B21 antibody upregulated the levels of proteins which cause cell cycle arrest and cell death such as TRAIL R1/DR4 and TRAIL R1/DR5, P21, BAX, p27/Kip1, and cleaved caspase 3; whereas inhibited the levels of pro-survival proteins such as BCl2 and BClxL. In contrast, B14 antibody upregulated only p27 and cleaved caspase-3 in our selected time point, whereas it reduced the levels of BCL2 and BCLxL more than B21 antibody (Supplementary Fig. S13C and S13D). These findings were further corroborated by Annexin V FITC/PI assay using flow cytometry, which also showed a significant increase in early and late apoptotic cells after treatment with B14 and B21 anti-OSMR antibodies in the presence of OSM for 16h (Fig. 4G and Supplementary Fig. S14A and S14B).

Next, we validated the levels of several oncogenic kinases that were inhibited in the protein kinase array by the treatment of B14 and B21 mAbs using immunoblot and found that B14 and B21 treatments reduced the levels of phospho-STAT3 proteins and pro survival markers such as PCNA and BCL-xL. We also observed that B14 and B21 mAbs improved the levels of apoptotic markers cytochrome c and p27 (Supplementary Fig. S14C and S14D). In consistent with phospho-protein array data (Fig. 4F), our immunoblot also showed that B14 and B21 antibodies reduced the level of phosphorylation of JAK1 (Y1034/1035) and JAK-2 (Y1007/1008), p85 subunit of PI3K (Y458), AKT (S473) and ERK (T202/Y204) (Supplementary Fig. S14E). To further evaluate the anti-cancer effects of B14, and B21 antibodies *in vitro*, we examined their effects on spheroid forming ability in HEYA8 cells and colony formation in both OVCAR4 and HEYA8 cells and found that B14 and B21 antibodies reduced the colony forming 3D morphogenesis abilities of OVCAR4 and HEYA8 cells (Supplementary Fig. S14F and S14G). Notably, B14 and B21 mAbs inhibited the key markers of ovarian cancer stemness such as CD133 (Prominin), CD44, CD113 (c-KIT) and ALDH1 in HEYA8 cells (Supplementary Fig. S14H).

To confirm that the effects observed in ovarian cancer cells upon anti-OSMR antibody, are operated through OSMR and its downstream target STAT3, we treated the most effective anti-OSMR antibody clone in HEYA8 cells that were knocked down for OSMR. As expected, B21 mAb was only effective in the control cells, whereas B21 mAb did not reduce the viability, spheroid formation ability, migration and colony formation of OSMR-depleted cells (Supplementary Fig. S15A to S15C). In conjunction, levels of OSMR and phosphorylation of STAT3 were reduced upon B21 treatment in the control cells but was not altered in HEYA8-shOSMR cells (Supplementary Fig. S15D).

Anti-OSMR antibody abrogated the dimerization of OSMR and promoted the internalization and degradation of OSMR in ovarian cancer cells

To investigate whether B14 and B21 monoclonal antibodies (mAbs) inhibit OSM-induced dimerization of OSMR with IL6ST, we immunoprecipitated OSMR-IL6ST heterodimer complex cross-linked after treating with anti-OSMR antibody or control IgG. Of note, we found that B14 and B21 abrogated the dimerization between OSMR and IL6ST considerably in both HEYA8 and OVCAR4 cells (Fig. 5A). Of note, B14 and B21 mAb treatment did not affect the dimerization of OSMR with IL31RA induced by IL31 when OSMR was immunoprecipitated (Supplementary Fig. S15E). Next, we confirmed if the treatment of B14 and B21 antibodies change the level of OSMR expression on cell membrane by on-cell Western assay. Here, we assessed the binding of B14 and B21 antibodies on the extracellular domain of OSMR in ovarian cancer cells by treating OVCAR4 and HEYA8 cells with control IgG, B14 or B21 in the presence of OSM for 16h. Cells were then fixed and immunostained using a second and a commercially available anti-OSMR antibody labelled with IR Dye-680RD (red fluorescence) antibody and quantitated the level of OSMR on cell surface. In this assay, we found that the treatment of B14 and B21 mAbs considerably reduced the presence of intact OSMR on the surface of both HEYA8 and OVCAR4 ovarian cancer cells (Fig. 5B and 5C), potentially due to the internalization and degradation of OSMR.

Thus, we decided to further confirm if the binding of B14 and B21 mAbs could mediate the internalization and degradation of OSMR by immunoblotting OSMR and its dimerizing partner IL6ST using the cytoplasmic and membrane fractions isolated from HEYA8 ovarian cancer cells, which were treated with B14 and B21 antibodies in the presence of OSM. Strikingly, our results showed that both B14 and B21 promoted the internalization of OSMR to cytoplasm (Fig. 5D and Supplementary Fig. S15F). We then validated the antibody mediated OSMR internalization in a complimentary approach, where we employed the Incucyte Live cell Analyzer to monitor internalization of OSMR from cell surface to cytoplasm in real time. Here we used B14 and B21 mAbs that were pre-labeled with pH sensitive Incucyte FabFluor red reagent. In contrast to the extracellular pH at ~7.4 (neutral pH), the FabFluor red labeled antibody produce red fluorescence when OSMR-labeled antibodies internalized into the cytoplasm or when localized to endosomes or lysosomes where the pH is acidic (~4.7 to 6.3) (Fig. 5E). In complement to our results that B14 and B21 reduced the quantity of intact OSMR on cell surface and promoted its internalization (Fig. 5B and 5C), our FabFluor red labeled antibody-based assay demonstrated that both B14 and B21 antibodies induced internalization of OSMR from cell surface to cytoplasm ~12h after treatment in both HEYA8 and OVCAR4 cells (Fig. 5F and 5G and Supplementary Fig. S15G and S15H). Next, we performed confocal microscopy on OVCAR4 cells that were treated with control IgG, B14 and B21 in the presence of OSM and immunostained with OSMR and LAMP1 (lysosomal marker). We found that B14 and B21 antibody treatments compared to the control IgG promoted internalization of OSMR into cytoplasm and colocalization with LAMP1 as an indication of lysosomal degradation (Fig 5 H). Taken together, our results demonstrate that the treatment of both B14 and B21 anti-OSMR antibodies blocked the binding of OSM to OSMR and its dimerization with

IL6ST receptor. In consequence, we observed that B14 and B21 anti-OSMR antibodies promoted the internalization and degradation of OSMR.

In vivo delivery of anti-OSMR antibodies reduced the growth and peritoneal spread of ovarian cancer cells

To evaluate the therapeutic effects of B14 and B21 anti-OSMR mAbs *in vivo*, we injected our *in vitro* validated anti-OSMR antibodies in athymic nude mice in which HEYA8 ovarian cancer cells were inoculated intraperitoneally with stably expressing luciferase reporter. Mice were treated with either control IgG, B14 or B21antibodies (10mg/kg body weight) 7^{th} day after cancer cell inoculation intraperitoneally twice a week. Because the mouse derived OSM does not bind to the human OSMR (30), these mice were supplemented with recombinant human OSM (250 ng/kg body weight) twice/week intraperitoneally along with B14 and B21 antibody treatment. All the mice were monitored for the growth of cancer cells by bioluminescence imaging for five weeks (Fig. 6A). The treatment of exogenous OSM promoted the growth of ovarian cancer cells *in vivo* (Fig. 6B and 6C). In agreement with our *in vitro* finding, treatment of B14 and B21 antibodies reduced the overall burden of cancer cells, number of tumor nodules and incidence of metastasis compared to mice that were either treated with control IgG antibody alone or the mice received exogenous OSM along with control IgG (Fig. 6B to 6F). Notably, our survival analysis demonstrated that the mice bearing HeyA8 cells treated with B14 and B21 exhibited a better overall survival (log rank test p-value < 0.0001) with a median survival of ~60 days and more than 100 days respectively as compared to Isotype control IgG treated mice (Fig. 6G). In contrast, OSM stimulated mice along with control IgG antibody exhibited poor survival with median survival of 29 days as compared to Control IgG treated group alone (Fig. 6G). Our immunohistochemistry analysis and/or Western blotting using the cancer tissues collected from Fig. 6B, showed that B21 antibody treatment was more effective than B14 antibody in reducing OSMR, pSTAT3 expression, proliferation marker Ki67 and anti-apoptotic marker BCLxl as compared to control IgG with and without OSM treated mice (Fig. 6H and 6I and Supplementary Fig. S16A). We also found that B21 antibody treatment upregulated the levels of cell death marker cleaved caspase-3 in the cancer tissues as compared to OSM stimulated group, or when compared to B14 antibody group or control IgG group with and without OSM (Fig. 6H and 6I). Of note, we did not find any unfavorable toxicity in the mice when treated with our antibody clones as exemplified by no significant change in body weight, alanine aminotransferase (ALT), aspartate aminotransferase (AST), bilirubin, albumin, creatine kinase, total protein levels and the histopathology of organs (kidney, liver, lung, heart, brain and spleen) in all the treatment groups (Supplementary Table. S5 and Supplementary Fig. S16B). Taken together, our *in vitro* and *in vivo* models along with validation of toxicity studies provide evidence that the treatment of B14 and B21 anti-OSMR antibodies will have the potential to use a therapeutic strategy to treat ovarian cancers, which express OSMR.

Discussion

Earlier studies of the OSMR family gene network were primarily focused on the signaling mechanisms regulated by OSM and/or OSMR (12,31). In contrast, the potential of

developing OSMR as a therapeutic target has not been sufficiently explored. In this study, we have determined the role of all IL6 family receptors in ovarian cancer and found that OSMR is an important therapeutic liability compared to other members of IL6 family receptors in ovarian cancer. Using the power of single-cell sequencing, cell biology and biochemical approaches, we found OSMR is expressed predominantly in ovarian cancer cells and a targetable receptor for therapy. There are three ligands such as OSM, IL31 and LIF can interact with OSMR. Our assays demonstrated that OSM is the key ligand which causes STAT3 activation for prolonged period support the notion that OSM provide robustness to oncogenic signaling.

Consistent with our results, others have also reported that stromal cells such as dendritic cells, macrophages and neutrophil populations are rich sources of secreted OSM (32–34). Studies have also demonstrated that the treatments of chemotherapeutic agent like cisplatin induces OSM levels suggests that OSMR-signaling could be key mechanism for cisplatin resistance (35,36). Importantly, OSM induces the dimerization of OSMR with another receptor partner IL6ST. Studies have also demonstrated that the treatments of chemotherapeutic agent like cisplatin induces OSM levels suggests that OSMR-signaling is a key mechanism for cisplatin resistance, which is a common scenario that severely affects the treatment efficacy in ovarian cancer patients (35,36). Thus, an agent that could abrogate the binding of OSM to OSMR and its dimerization with IL6ST could inhibit tumor progression particularly the most aggressive ovarian cancers including cisplatin-resistant ovarian cancer.

In this study, we address three paradigms, which are critical for the growth and progression of ovarian cancer: (i) a paradigm of oncogenic addiction operating through elevated levels of OSMR on ovarian cancer cells and its ligand OSM produced by stromal cells. (ii) a paradigm of downstream oncogenic signaling mediated through STAT3 activated by OSMR and its dimerization with IL6ST upon OSM binding, and (iii) a paradigm of blocking OSMR dimerization with IL6ST and subsequent oncogenic signaling using target-specific anti-OSMR antibodies.

Towards the goal of treating ovarian cancer patients as a feasible therapeutic approach, we developed a set of anti-OSMR antibodies and tested the efficacy of these antibodies in inhibiting the oncogenic signaling mediated through STAT3, tumor cell growth and metastasis both *in vitro* and/or *in vivo*. Importantly, the antibody we developed was able to prevent the dimerization of OSMR with IL6ST and by promoting its internalization and degradation in cancer cells. In contrast to hematological cancers and other solid malignancies such as breast and colorectal cancer, monoclonal antibodies (mAbs)-based therapy has not been proven to be effective for the treatment of ovarian cancer.

Several mAbs have been developed and approved by the FDA for solid tumors. One of them being the widely used Trastuzumab (a.k.a. Herceptin), which is very similar to the kind of antibody we have developed in terms of inhibiting heterodimerization of receptors. Trastuzumab is a humanized monoclonal antibody raised against the extracellular domain of HER2 (ERBB2) and is known for inhibiting the ligand-independent hetero-dimerization between ERBB2 and other EGFR family members by binding to the extracellular domain

of HER2 (ERBB2) (37). It is reported that antibodies bind to transmembrane receptors may block their binding to ligands and promotes receptor internalization and degradation (15). According to this notion, the binding of B14 and B21 antibody to OMSR receptors were also blocked the OSMR dimerization, then induced OSMR internalization potentially by recognizing endocytic machinery, then sorting OSMR into lysosomes for degradation. These effects of our antibody clones were culminated into a reduction in phosphorylation and activation of downstream effectors such as STAT3, PI3K-Akt-mTOR and MEK-ERK proteins, which are critical survival mechanisms in tumor cells.

Therapeutic antibodies have also been implicated in the induction of apoptosis via intrinsic (or mitochondrial) pathway, leading to cytochrome release from mitochondria, downregulation of MAP-kinase and Akt pathways, anti-apoptotic Bcl-2 family proteins, and upregulation of cyclin-dependent kinases (CDK) inhibitors (38,39). Similar to these findings, our antibody clones B14 and B21 antibody clones inhibited the levels of BCl_2, and upregulated the levels of p27, cleaved caspase-3, TRAIL receptors and cytochrome-c. Likewise, the treatment of B14 and/or B21 reduced the growth and peritoneal spread of ovarian cancer cells *in vivo,* where the treatment inhibited the levels of OSMR, phosphorylated STAT3, BCL-xL and induced the levels of cleaved caspase-3.

Monoclonal antibodies can specifically target cancer cells while avoiding healthy cells and can also harness the body's own immune system to fight cancer with substantially fewer devastating side-effects than more conventional chemotherapy or radiotherapy. Overall, the use of human antibodies revolutionized therapeutics. We expect that our anti-OSMR antibody can specifically target ovarian cancer cells without harming healthy normal cells. Further engineering or refinement may be required for enhancing their binding to its target and provide better efficacy, currently undergoing in our laboratory. OSMR is also highly expressed in other cancers like cervical, lung, and renal cancers. Thus, anti-OSMR antibodies are expected to be beneficial for treating a broader number of cancers that depend on OSMR signaling as a critical mechanism for their growth and progression.

Supplementary Material

Refer to Web version on PubMed Central for supplementary material.

Acknowledgement

This work was supported in part by funding from NCI R01CA229907 to P.C.-R., the Ovarian Cancer Research Fund Alliance (OCRFA; P.C.R., S.P.), the Women's Health Research Program (WHRP), the Sharon L. La Macchia Innovation Fund at MCW, MCW Cancer Center Institutional Research Grants from the American Cancer Society (16-183-31 to P.C.-R., 14-247-29 to Y.S.) and seed grants from MCW Cancer Center. Z.A. was supported in part by a Welch Foundation grant AU-0042-20030616 and Cancer Prevention and Research Institute of Texas (CPRIT) Grants RP150551 and RP190561.

MBD was supported in part by grants from the National Cancer Institute R01 CA226279 and continuing philanthropic support from the Bobbie Nick Voss Charitable Foundation. J.S.R. was supported by the NCI R21CA241013.

References

1. Coward JI, Middleton K, Murphy F. New perspectives on targeted therapy in ovarian cancer. Int J Womens Health 2015;7:189–203 [PubMed: 25678824]
2. Siegel RL, Miller KD, Jemal A. Cancer statistics, 2018. CA Cancer J Clin 2018;68:7–30 [PubMed: 29313949]
3. Torre LA, Trabert B, DeSantis CE, Miller KD, Samimi G, Runowicz CD, et al. Ovarian cancer statistics, 2018. CA Cancer J Clin 2018;68:284–96 [PubMed: 29809280]
4. Izar B, Tirosh I, Stover EH, Wakiro I, Cuoco MS, Alter I, et al. A single-cell landscape of high-grade serous ovarian cancer. Nat Med 2020;26:1271–9 [PubMed: 32572264]
5. Parashar D, Geethadevi A, Aure MR, Mishra J, George J, Chen C, et al. miRNA551b-3p Activates an Oncostatin Signaling Module for the Progression of Triple-Negative Breast Cancer. Cell Rep 2019;29:4389–406 e10 [PubMed: 31875548]
6. Rose-John S Interleukin-6 Family Cytokines. Cold Spring Harb Perspect Biol 2018;10
7. Chaluvally-Raghavan P, Jeong KJ, Pradeep S, Silva AM, Yu S, Liu W, et al. Direct Upregulation of STAT3 by MicroRNA-551b-3p Deregulates Growth and Metastasis of Ovarian Cancer. Cell reports 2016;15:1493–504 [PubMed: 27160903]
8. Yoshikawa T, Miyamoto M, Aoyama T, Soyama H, Goto T, Hirata J, et al. JAK2/STAT3 pathway as a therapeutic target in ovarian cancers. Oncol Lett 2018;15:5772–80 [PubMed: 29545902]
9. Zou S, Tong Q, Liu B, Huang W, Tian Y, Fu X. Targeting STAT3 in Cancer Immunotherapy. Mol Cancer 2020;19:145 [PubMed: 32972405]
10. Taga T, Kishimoto T. Gp130 and the interleukin-6 family of cytokines. Annu Rev Immunol 1997;15:797–819 [PubMed: 9143707]
11. Murakami M, Kamimura D, Hirano T. Pleiotropy and Specificity: Insights from the Interleukin 6 Family of Cytokines. Immunity 2019;50:812–31 [PubMed: 30995501]
12. Tanaka M, Miyajima A. Oncostatin M, a multifunctional cytokine. Rev Physiol Biochem Pharmacol 2003;149:39–52 [PubMed: 12811586]
13. Demyanets S, Kaun C, Rychli K, Pfaffenberger S, Kastl SP, Hohensinner PJ, et al. Oncostatin M-enhanced vascular endothelial growth factor expression in human vascular smooth muscle cells involves PI3K-, p38 MAPK-, Erk1/2- and STAT1/STAT3-dependent pathways and is attenuated by interferon-gamma. Basic Res Cardiol 2011;106:217–31 [PubMed: 21174212]
14. Kurosawa T, Yamada A, Takami M, Suzuki D, Saito Y, Hiranuma K, et al. Expression of nephronectin is inhibited by oncostatin M via both JAK/STAT and MAPK pathways. FEBS Open Bio 2015;5:303–7
15. Ben-Kasus T, Schechter B, Lavi S, Yarden Y, Sela M. Persistent elimination of ErbB-2/HER2-overexpressing tumors using combinations of monoclonal antibodies: relevance of receptor endocytosis. Proceedings of the National Academy of Sciences of the United States of America 2009;106:3294–9 [PubMed: 19218427]
16. Goldberg RM. Cetuximab. Nat Rev Drug Discov 2005;Suppl:S10–1 [PubMed: 15962524]
17. Smyth EC, Tarazona N, Chau I. Ramucirumab: targeting angiogenesis in the treatment of gastric cancer. Immunotherapy 2014;6:1177–86 [PubMed: 25496333]
18. Slyper M, Porter CBM, Ashenberg O, Waldman J, Drokhlyansky E, Wakiro I, et al. A single-cell and single-nucleus RNA-Seq toolbox for fresh and frozen human tumors. Nat Med 2020;26:792–802 [PubMed: 32405060]
19. Chen C, Gupta P, Parashar D, Nair GG, George J, Geethadevi A, et al. ERBB3-induced furin promotes the progression and metastasis of ovarian cancer via the IGF1R/STAT3 signaling axis. Oncogene 2020;39:2921–33 [PubMed: 32029900]
20. Efremova M, Vento-Tormo M, Teichmann SA, Vento-Tormo R. CellPhoneDB: inferring cell-cell communication from combined expression of multi-subunit ligand-receptor complexes. Nat Protoc 2020;15:1484–506 [PubMed: 32103204]
21. Parashar D, Nair B, Geethadevi A, George J, Nair A, Tsaih SW, et al. Peritoneal Spread of Ovarian Cancer Harbors Therapeutic Vulnerabilities Regulated by FOXM1 and EGFR/ERBB2 Signaling. Cancer Res 2020;80:5554–68 [PubMed: 33087324]

22. Romano G, Chen PL, Song P, McQuade JL, Liang RJ, Liu M, et al. A Preexisting Rare PIK3CA(E545K) Subpopulation Confers Clinical Resistance to MEK plus CDK4/6 Inhibition in NRAS Melanoma and Is Dependent on S6K1 Signaling. Cancer Discov 2018;8:556–67 [PubMed: 29496665]
23. Turk HF, Chapkin RS. Analysis of epidermal growth factor receptor dimerization by BS(3) cross-linking. Methods Mol Biol 2015;1233:25–34 [PubMed: 25319886]
24. Bublil EM, Pines G, Patel G, Fruhwirth G, Ng T, Yarden Y. Kinase-mediated quasi-dimers of EGFR. FASEB journal : official publication of the Federation of American Societies for Experimental Biology 2010;24:4744–55 [PubMed: 20682838]
25. Phuchareon J, McCormick F, Eisele DW, Tetsu O. EGFR inhibition evokes innate drug resistance in lung cancer cells by preventing Akt activity and thus inactivating Ets-1 function. Proc Natl Acad Sci U S A 2015;112:E3855–63 [PubMed: 26150526]
26. Parashar D, Geethadevi A, McAllister D, Ebben J, Peterson FC, Jensen DR, et al. Targeted biologic inhibition of both tumor cell-intrinsic and intercellular CLPTM1L/CRR9-mediated chemotherapeutic drug resistance. NPJ Precis Oncol 2021;5:16 [PubMed: 33654182]
27. Subramanian A, Tamayo P, Mootha VK, Mukherjee S, Ebert BL, Gillette MA, et al. Gene set enrichment analysis: a knowledge-based approach for interpreting genome-wide expression profiles. Proc Natl Acad Sci U S A 2005;102:15545–50 [PubMed: 16199517]
28. Liberzon A, Birger C, Thorvaldsdottir H, Ghandi M, Mesirov JP, Tamayo P. The Molecular Signatures Database (MSigDB) hallmark gene set collection. Cell Syst 2015;1:417–25 [PubMed: 26771021]
29. Ziegenhain C, Vieth B, Parekh S, Reinius B, Guillaumet-Adkins A, Smets M, et al. Comparative Analysis of Single-Cell RNA Sequencing Methods. Mol Cell 2017;65:631–43 e4 [PubMed: 28212749]
30. Adrian-Segarra JM, Sreenivasan K, Gajawada P, Lorchner H, Braun T, Poling J. The AB loop of oncostatin M (OSM) determines species-specific signaling in humans and mice. J Biol Chem 2018;293:20181–99 [PubMed: 30373773]
31. Richards CD. The enigmatic cytokine oncostatin m and roles in disease. ISRN Inflamm 2013;2013:512103
32. Pothoven KL, Norton JE, Suh LA, Carter RG, Harris KE, Biyasheva A, et al. Neutrophils are a major source of the epithelial barrier disrupting cytokine oncostatin M in patients with mucosal airways disease. J Allergy Clin Immunol 2017;139:1966–78 e9 [PubMed: 27993536]
33. Suda T, Chida K, Todate A, Ide K, Asada K, Nakamura Y, et al. Oncostatin M production by human dendritic cells in response to bacterial products. Cytokine 2002;17:335–40 [PubMed: 12061841]
34. Blanchard F, Wang Y, Kinzie E, Duplomb L, Godard A, Baumann H. Oncostatin M regulates the synthesis and turnover of gp130, leukemia inhibitory factor receptor alpha, and oncostatin M receptor beta by distinct mechanisms. J Biol Chem 2001;276:47038–45 [PubMed: 11602599]
35. Singh RA, Sodhi A. Cisplatin-treated macrophages produce oncostatin M: regulation by serine/threonine and protein tyrosine kinases/phosphatases and Ca2+/calmodulin. Immunol Lett 1998;62:159–64 [PubMed: 9698114]
36. Sodhi A, Shishodia S, Shrivastava A. Cisplatin-stimulated murine bone marrow-derived macrophages secrete oncostatin M. Immunol Cell Biol 1997;75:492–6 [PubMed: 9429898]
37. Nahta R, Hung MC, Esteva FJ. The HER-2-targeting antibodies trastuzumab and pertuzumab synergistically inhibit the survival of breast cancer cells. Cancer Res 2004;64:2343–6 [PubMed: 15059883]
38. Ben-Kasus T, Schechter B, Sela M, Yarden Y. Cancer therapeutic antibodies come of age: targeting minimal residual disease. Molecular oncology 2007;1:42–54 [PubMed: 19383286]
39. Cuello M, Ettenberg SA, Clark AS, Keane MM, Posner RH, Nau MM, et al. Down-regulation of the erbB-2 receptor by trastuzumab (herceptin) enhances tumor necrosis factor-related apoptosis-inducing ligand-mediated apoptosis in breast and ovarian cancer cell lines that overexpress erbB-2. Cancer Res 2001;61:4892–900 [PubMed: 11406568]

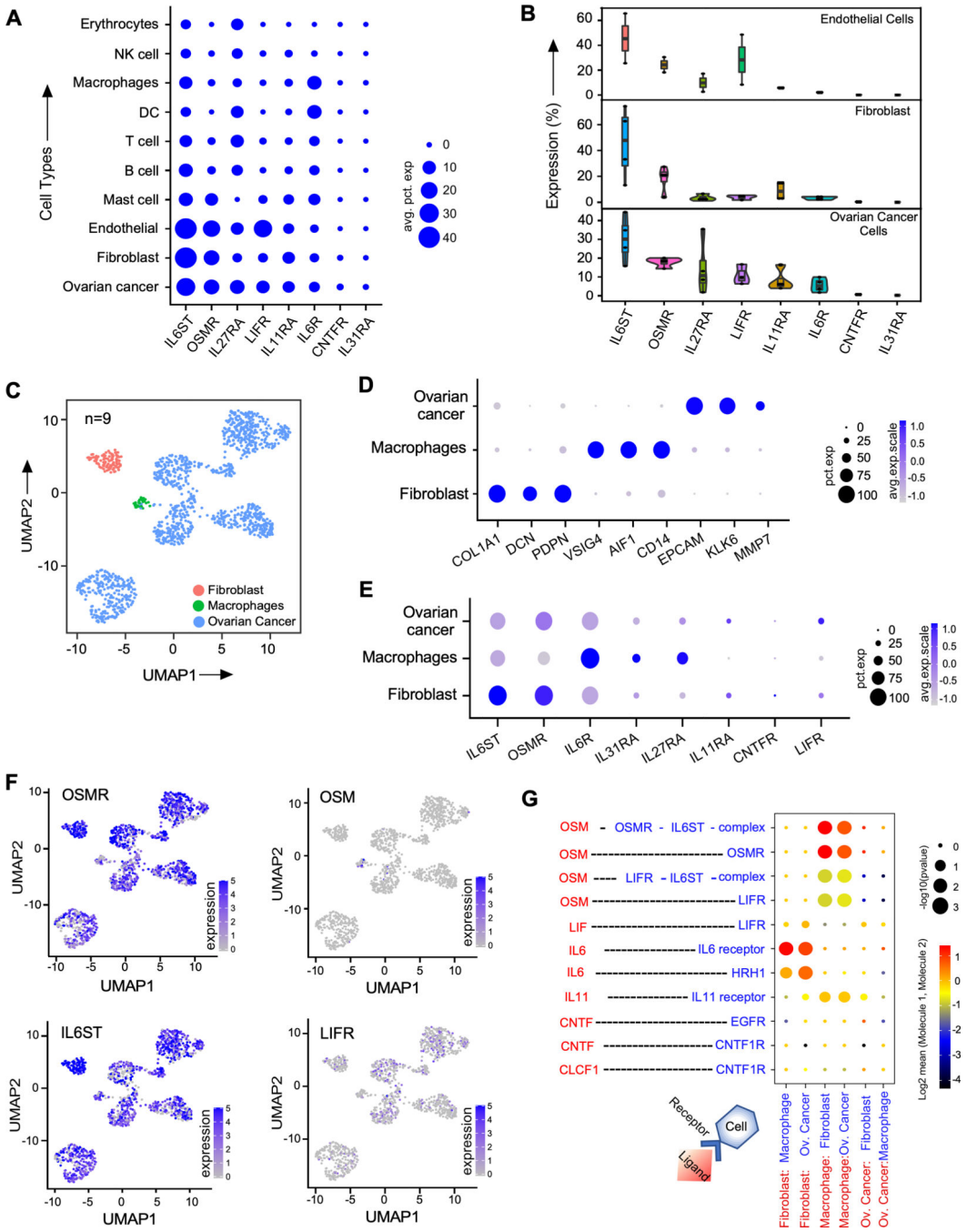

Figure. 1. OSMR is highly expressed in ovarian cancer cells.

A, Dot plot of average across the four 10x datasets of percent of cells expressing IL6 family receptors in different cell types. **B,** Violin box dot plots demonstrate the distribution of percent of cells expressing IL6 family receptors in ovarian cancer cells, fibroblasts and endothelial cells in the four 10x datasets. **C**, Different cell types detected in SS2 patient dataset (n=9). Uniform manifold approximation and projection (UMAP) embedding of single cells (dots), colored by cell types. **D**, Cell-type specific markers in SS2 dataset showing their prevalence and strength of expression. **E**, Expression of IL6 family receptors

in the different cell types in SS2 dataset. **F**, UMAP embedding of single cell colored (blue color) by expression of OSM, OSMR, and IL6ST. **G**, Ligand-receptor interactions detected for the IL6 family ligands (red color) and receptors or receptor complex (blue color) between the different cell types in SMART-seq2 scRNA-seq data (SS2) dataset. Size of dots represent percentage abundance of IL6 family receptors in the respective cell type.

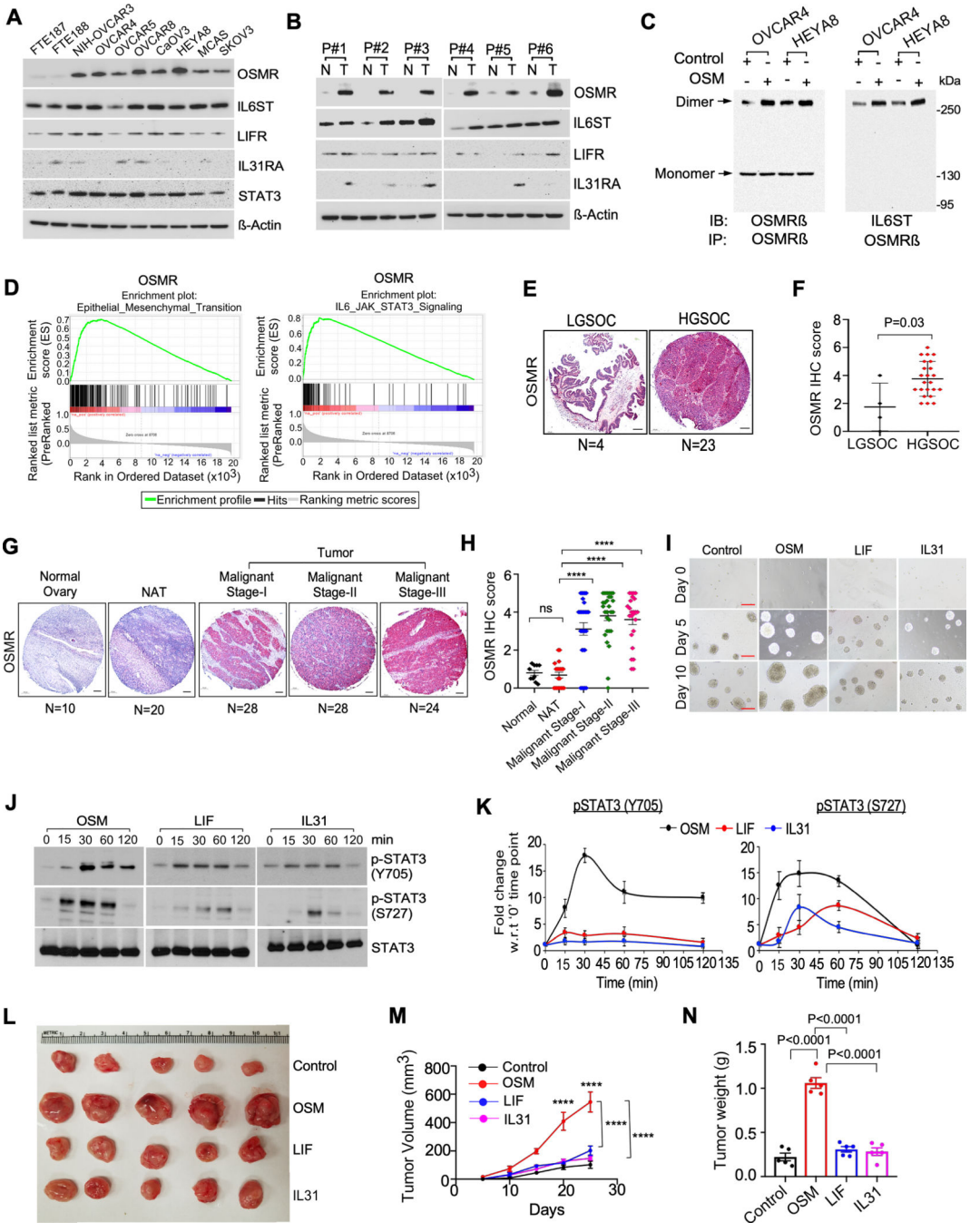

Figure. 2. OSM is critical for oncogenic signaling activation for prolonged period and ovarian cancer growth.

A, Western blot analysis of the indicated protein levels in normal fallopian tube epithelial cell lines (FTE187 and FTE188) and human ovarian cancer cell lines. β-Actin was used as a loading control. **B,** Western blot analysis of indicated proteins expressed in Ovarian cancer tissues (T) (n=6) from patients (P#1 to P#6) compared to normal adjacent ovarian tissues (N) (n=6). **C,** HEYA8 and OVCAR4 cells were stimulated with OSM (100ng/mL) for 1h. Cell lysates were prepared after crosslinking with BS3 reagent and immunoprecipitated

(IP) using anti-OSMR antibody, then resolved on SDS/PAGE. Dimers and monomers (arrows) were detected using an anti-OSMR and anti-IL6ST antibodies. **D,** GSEA analysis demonstrating the enrichment score of indicated functional annotation marks based on OSM expression in the TCGA ovarian cancer samples. ES: enrichment score, NES: normalized enrichment score. **E and G,** Representative immunohistochemistry (IHC) images and quantification of OSMR expression in the indicated sample groups in an ovarian cancer tissue microarray (TMA)-OV1005bt and OV1004; LGSOC= Low grade serous ovarian cancer, HGSOC= High grade serous ovarian cancer, NAT = normal adjacent tissue. Number (N) of tissue samples are indicated at the bottom of each image. **F and H,** OSMR staining intensity was scored and quantitated in each sample group. **I,** Representative images of 3D spheroids of HEYA8 cells grown in the presence of OSM (100ng/mL), LIF (100ng/mL) or IL31 (50ng/mL) at indicated days. Scale bar, 500μm. **J,** HEYA8 cells were treated with OSM (100ng/mL), LIF (100ng/mL) or IL31 (50ng/mL) for indicated time points, then cell lysates were prepared, and Western blot was performed using indicated antibodies. **K,** Densitometric analysis of phosphorylated STAT3 normalized with total STAT3 as in (j) performed in three biological replicates. **L,** Female athymic nude mice (nu/nu) were subcutaneously injected with HEYA8 ovarian cancer cells. Mice were then treated with OSM, LIF, or IL31 intraperitoneally (i.p) twice a week for four weeks. Tumor were excised on 25^{th} day and images were captured (n=5 mice per group) **M,** Tumor volume was calculated in each group from (l) at the indicated time points. **N,** Tumor weight were quantitated upon termination on 25^{th} day. Results in (**K**) are presented as the means ± SEM from three separate experiments and Student's t test (two tailed, unpaired) was performed to determine P-value. Dunnett's multiple comparison test were performed in **(H, M, N)**. Data represent means ± SEM. ****P≤ 0.0001, ***P≤0.001, **P≤0.01, *P≤0.05, ns: not significant.

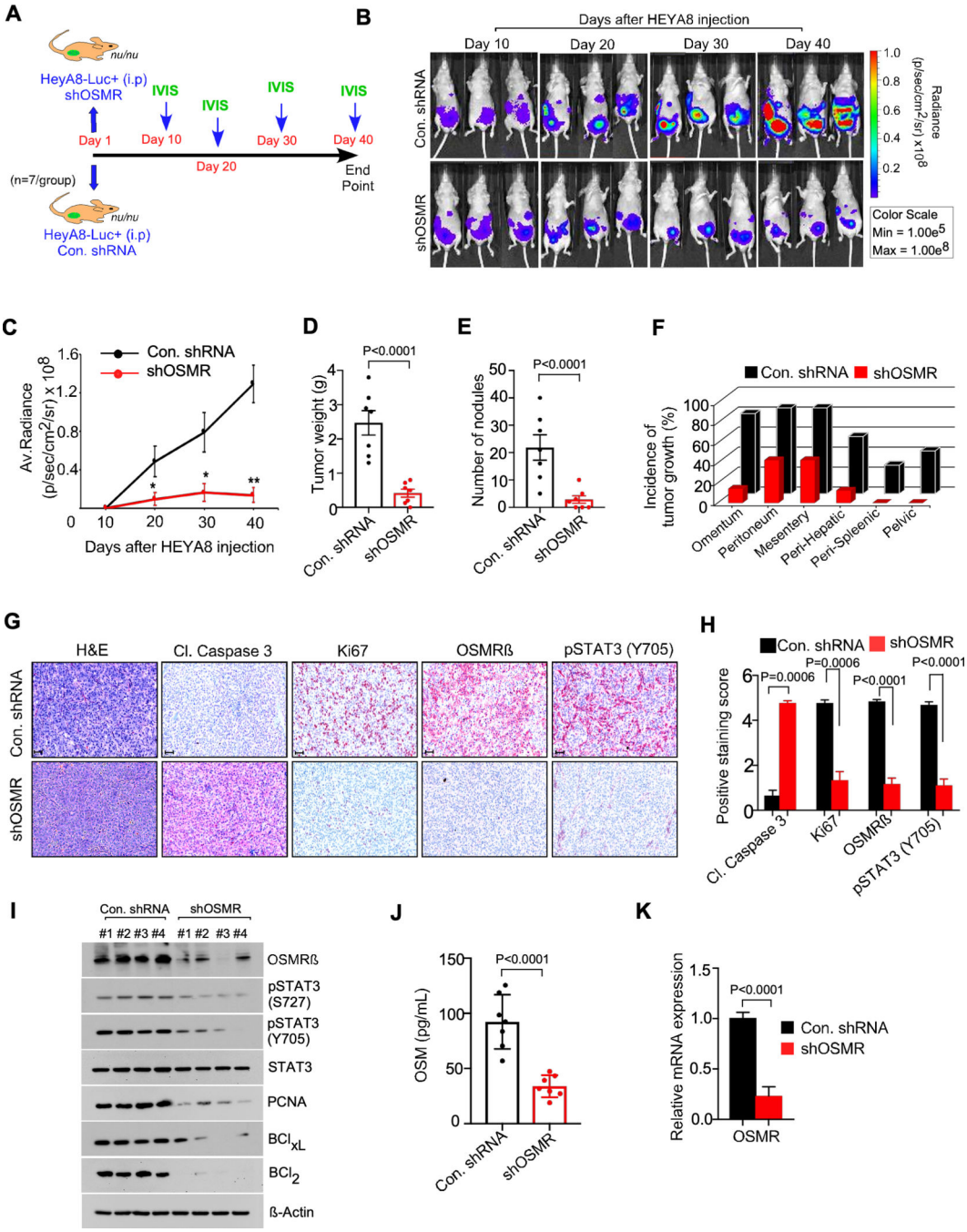

Figure. 3. OSMR knockdown reduced the growth and seeding of ovarian cancer cells *in vivo*.

A-C, Athymic female nude mice were injected with shControl-HEYA8-Luc+ cells intraperitoneally or shOSMR#1-HEYA8-Luc+ cells (n=7/group) and images were taken at the indicated days using IVIS100 bioluminescence imager. **D-F,** Mice from (b) were sacrificed at the end point (40th day) and total tumor weight, number of tumor nodules and the incidence of tumor growth were recorded. **G-H,** IHC of tumor tissues from (B) were performed using the antibodies indicated, then photographed and the antibody staining intensity was scored and quantitated. Scale bar, 50 μm. **I,** Three different tumor tissue lysates

from each group in (B) were immunoblotted. **J,** Serum from the mice in (A) were collected (n=7) and ELISA was performed to determine OSM levels. **K,** qPCR showing relative mRNA expression of OSMR in tumor tissues of mice from (b). Data represent means ± SEM and Student's t test (two tailed, unpaired) was performed to determine p-Value in **(C, D, E, H, J, K)**.

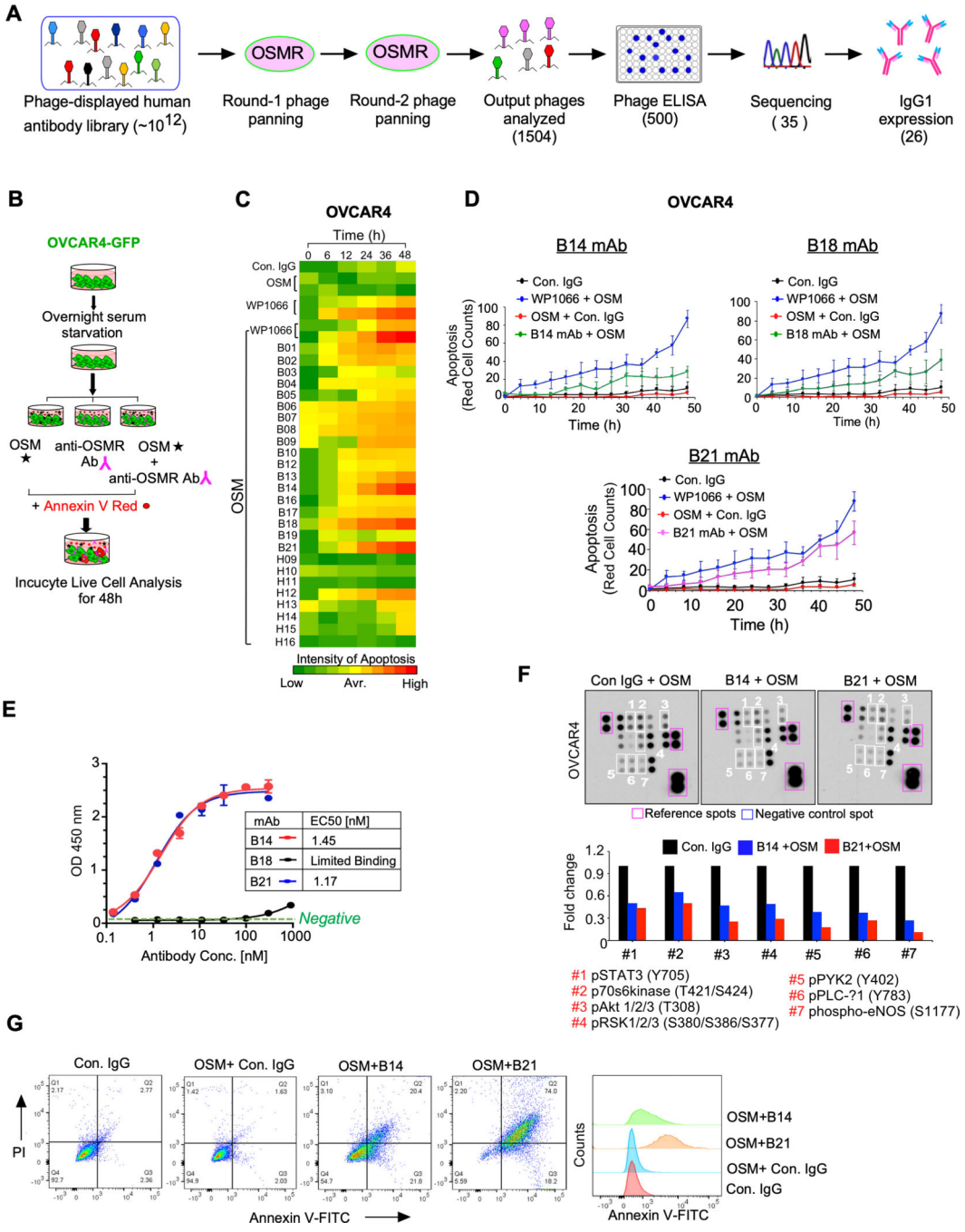

Figure. 4. Monoclonal antibody (mAb) of OSMR abrogates OSM-mediated oncogenic characteristics by blocking dimerization of OSMR.

A, Flowcharts demonstrate the scFv phage library panning and antibody selection process employed. **B,** Schema shows the flowchart of screening 26 anti-OSMR mAb by the ability to promote apoptosis in the presence of recombinant OSM (100ng/mL) in OVCAR4-GFP cells using Incucyte Live cell analyzer up to 48h. STAT3 inhibitor WP1066 was used as a positive control of apoptosis. **C,** OVCAR4 cell death induced by the antibody clones were evaluated by quantitating Annexin V positive cells using Incucyte Live cell analyzer at indicated time

points in triplicates. **D,** Rate of cell death induced by control IgG, B14, B18 and B21 mAbs from (C) were plotted. Data shown here is the mean of three fields per well and the assay was performed in as three biological and three technical replicates. **E,** Comparative binding affinities of purified B14, B18 and B21 anti-OSMR monoclonal antibodies with OSMR as determined by ELISA and the EC50 of mAb were determined. **F,** OVCAR4 cells were treated with B14 and B21 anti-OSMR antibodies in the presence of OSM for 24h and cell lysates were prepared, and the levels of phospho-kinase proteins from the protein array membrane (upper panel) were quantitated and presented as histograms. Each bar represents the mean of densitometry values of the phospho proteins altered on membrane (white squares). **G,** HEYA8 cells were pre-treated with B14 or B21 monoclonal antibodies for 4h, then stimulated with OSM (100ng/mL) for 16 h. Apoptosis was determined by Annexin V-FITC/PI staining using Flow cytometry. Data represent means ± SEM.

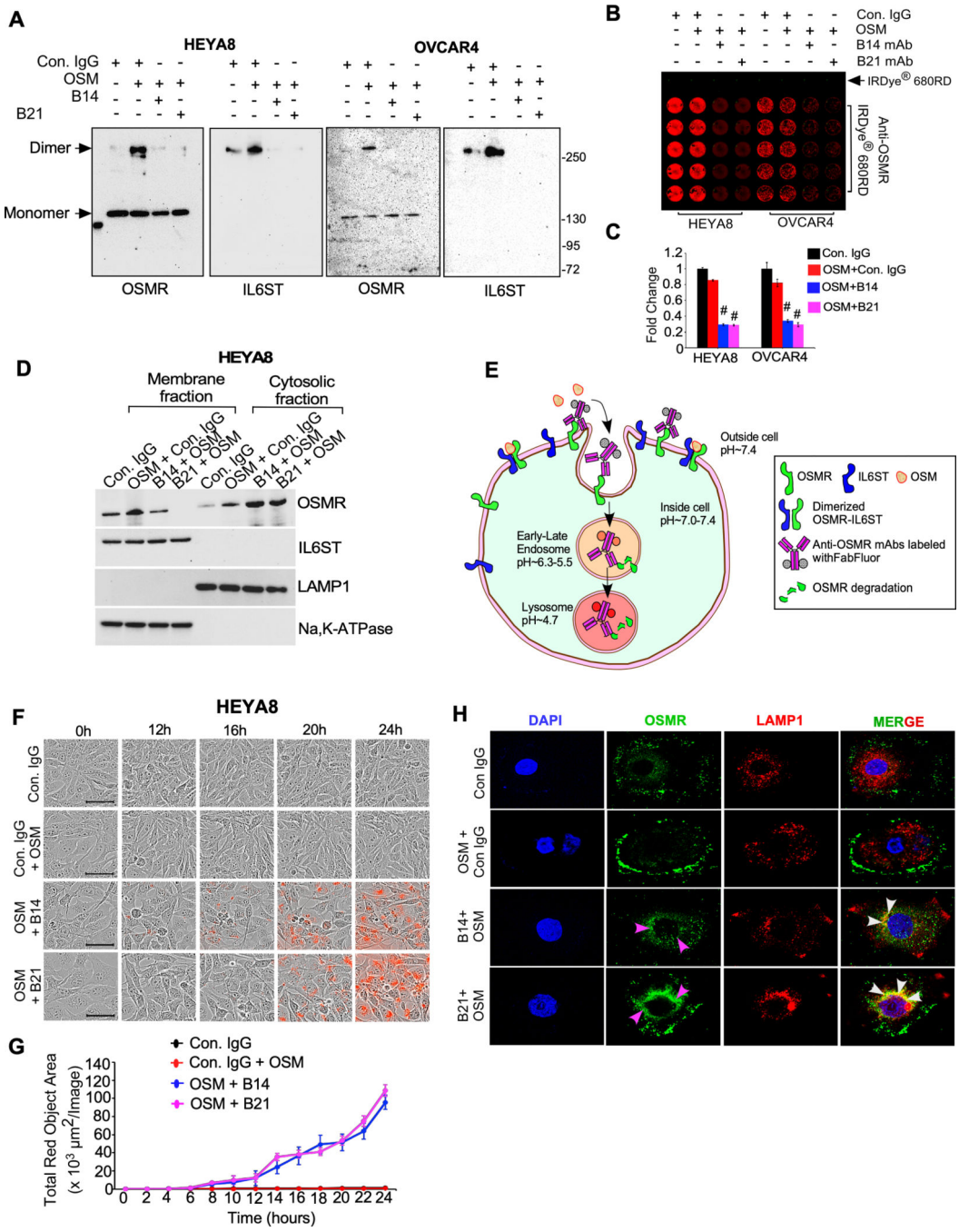

Figure. 5. Anti-OSMR antibodies abrogate heterodimerization of OSMR with IL6ST and induce internalization and degradation of OSMR.

A, HEYA8 and OVCAR4 cells were treated with B14 or B21 mAbs for 4h, then stimulated with OSM (100ng/mL) for 1h. Cell lysates were prepared after crosslinking with BS3 reagent and immunoprecipitated (IP) using anti-OSMR antibody, then resolved on SDS/ PAGE. Dimers and monomers (arrows) were then detected using an anti-OSMR and anti-IL6ST antibodies. **B,** In-cell western blotting of OSMR in HEYA8 and OVCAR4 cells were treated with Control IgG, B14 and B21 mAbs in the presence of OSM for 24h. Primary

antibodies bound on the cells were then labelled using secondary antibody 680RD infra-red dye and photographed. **C,** Each experiment was carried out in 5 biological and 3 technical replicates and fluorescent signals from (b) were quantified. **D,** HEYA8 cells were treated with B14 and B21 mAbs in the presence of OSM (100ng/mL) for 16h, then membrane and cytoplasmic fractions of cells were prepared, and Western blot was performed. LAMP1 and Na,K-ATPAse were used as internal controls of cytosolic and membrane fractions respectively. **E,** A schema depicts the process of anti-OSMR antibody mediated receptor internalization and degradation in cancer cells. Control IgG or B14 or B21 mAbs were labeled with Incucyte® Human FabFluor-pH Red Antibody Labeling Reagent and then added to cells along with OSM (100 ng/mL) and incubated for 24h. Red fluorogenic signals released due to the low-acidic pH when the FabFluor-labelled anti-OSMR antibody internalized to lysosomes were quantitated. **F,** HEYA8 cells were plated as described in (E) and time lapse imaging were performed to detect the fluorescence. Scale bar, 50μm. **G,** Quantitative assessment of internalized OSMR antibody complex based on the total red dot area per image as evaluated using Incucyte S3 software. **H,** Representative images of OSMR internalization and colocalization with LAMP1 lysosomal marker confocal microscopy. OVCAR4 cells were treated with control IgG, B14 and B21 mAbs in the presence of OSM for 16h and fixed and stained with OSMR-Alexa Fluor 488 (green) and LAMP1-Alex fluor 546 (red). Nuclei were stained with DAPI (blue). Student's t test (two tailed, unpaired) was performed to determine P-value. Data represent means ± SEM. $^{\#}P \leq 0.0001$.

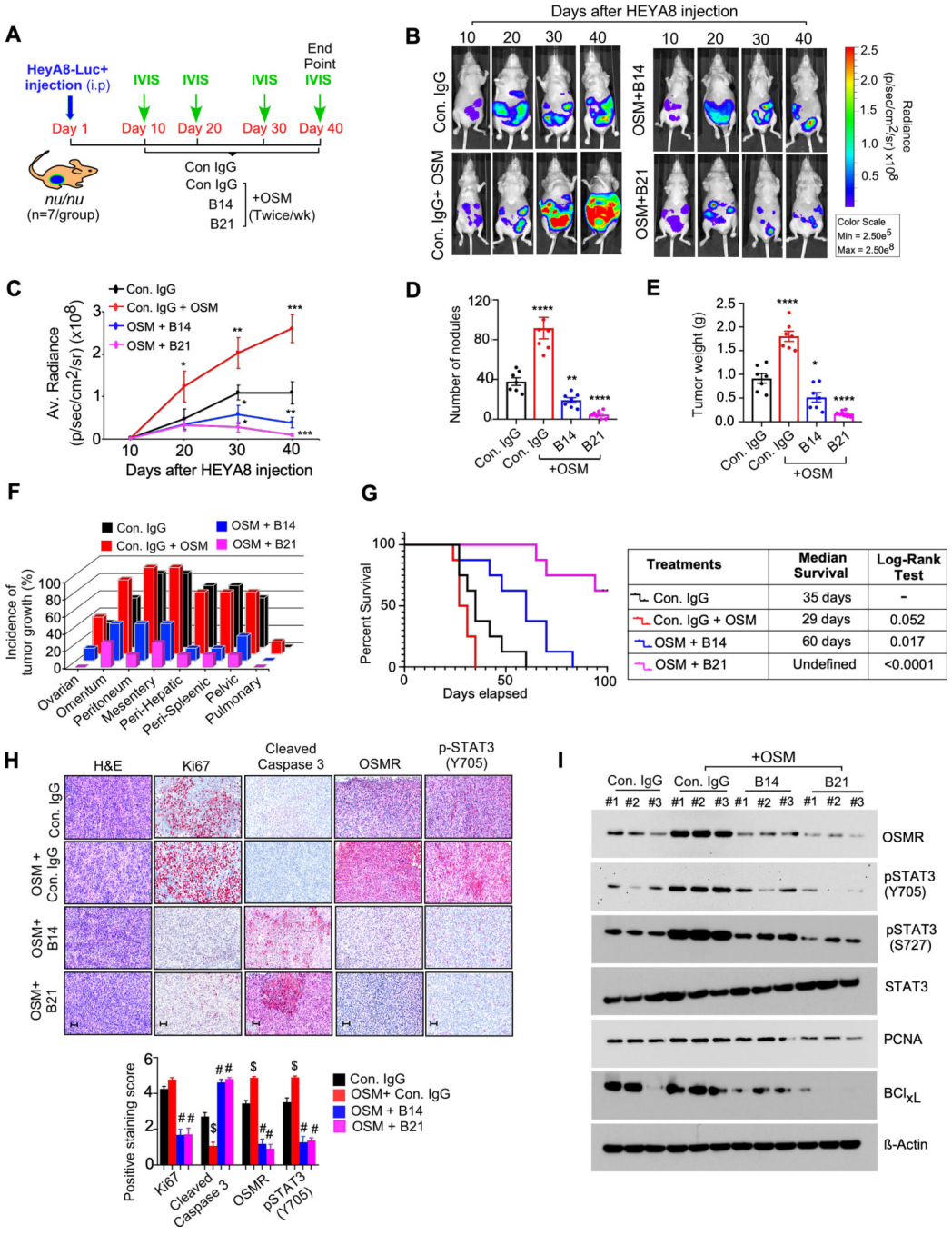

Figure. 6. Anti-OSMR antibodies reduced OSM mediated tumor growth and metastasis and improved overall survival rate of mice bearing ovarian cancer.

A, Schematic representation shows the experimental plan in athymic nude mice (nu/nu) injected with HEYA8-Luc+ cells intraperitoneally. Mice were treated with OSM (250 ng/kg body weight) 30 min after the injections of control IgG, B14, B21, antibodies (10mg/kg body weight) intraperitoneally for 5 weeks (N=7/ group) and then sacrificed. **B-C,** Representative images of tumor bearing mice were captured using an IVIS100 bioluminescence imager at the days indicated and the luminescence of tumor growth were

quantitated. **D-F,** Number of tumor nodules, total tumor weight and incidence of tumor growth in specific organ sites were determined at the end of the experiment. **G,** Overall survival rate of ovarian cancer bearing nu/nu mice treated with control IgG, OSM, OSM+ B14 or OSM + B21 anti-OSMR antibodies twice per week for a period of 5 weeks (n=10/ group) and rate of survival was determined for a total of ~15 weeks (>100 days). Log-rank test was performed to determine P-value by comparing each group with control IgG group. **H,** Representative H&E-stained sections and IHC of indicated proteins in tumor tissues, that were isolated from mice in **'**B**'** at the end of the experiment. Scale bar, 50 μm. **i** Western blots showing the expression of indicated proteins from three representative tumor tissues that were isolated from **'**a' at the end of the experiment. Data represent means ± SEM. Student's t test (two tailed, unpaired) and Dunnett's multiple comparison tests were performed to determine P-Value in **C, D, E and H**. ****P≤ 0.0001, ***P≤0.001, and *P≤0.05, $^{\#}$P≤ 0.0001, $^{\$}$≤ 0.0001